Title

KamLAND's search for correlated low-energy electron antineutrinos with astrophysical neutrinos from IceCube

Authors

Abe, S
Asami, S
Eizuka, M
et al.

Publication Date

2022-02-15

KamLAND's search for correlated low-energy electron antineutrinos with astrophysical neutrinos from IceCube

S. Abe[a], S. Asami[a], M. Eizuka[a], S. Futagi[a], A. Gando[a], Y. Gando[a], T. Gima[a], A. Goto[a], T. Hachiya[a], K. Hata[a], K. Hosokawa[a], K. Ichimura[a], S. Ieki[a], H. Ikeda[a], K. Inoue[a,e], K. Ishidoshiro[a], Y. Kamei[a], N. Kawada[a], Y. Kishimoto[a,e], T. Kinoshita[a], M. Koga[a,e], M. Kurasawa[a], N. Maemura[a], T. Mitsui[a], H. Miyake[a], T. Nakahata[a], K. Nakamura[a], K. Nakamura[a], R. Nakamura[a], H. Ozaki[a,c], T. Sakai[a], H. Sambonsugi[a], I. Shimizu[a], J. Shirai[a], K. Shiraishi[a], A. Suzuki[a], Y. Suzuki[a], A. Takeuchi[a], K. Tamae[a], H. Watanabe[a], Y. Yoshida[a], S. Obara[b], A. K. Ichikawa[d], S. Yoshida[f], S. Umehara[g], K. Fushimi[h], K. Kotera[h], Y. Urano[h], B. E. Berger[i,e], B. K. Fujikawa[i,e], J. G. Learned[j], J. Maricic[j], S. N. Axani[k], J. Smolsky[k], J. Lertprasertpong[k], L. A. Winslow[k], Z. Fu[k], J. Ouellet[k], Y. Efremenko[m,e], H. J. Karwowski[n,o], D. M. Markoff[n,p], W. Tornow[n,q,e], A. Li[o], J. A. Detwiler[r,e], S. Enomoto[r,e], M. P. Decowski[s,e], C. Grant[l], H. Song[l], T. O'Donnell[t], S. Dell'Oro[t]

[a] *Research Center for Neutrino Science, Tohoku University, Sendai, 980-8578, Japan*
[b] *Frontier Research Institute for Interdisciplinary Sciences, Tohoku University, Sendai, 980-8578, Japan*
[c] *Graduate Program on Physics for the Universe, Tohoku University, Sendai, 980-8578, Japan*
[d] *Department of Physics, Tohoku University, Sendai, 980-8578, Japan*
[e] *Institute for the Physics and Mathematics of the Universe, The University of Tokyo, Kashiwa, 277-8568, Japan*
[f] *Graduate School of Science, Osaka University, Toyonaka, 560-0043, Japan*
[g] *Research Center for Nuclear Physics (RCNP), Osaka University, Ibaraki, Osaka, 567-0047, Japan*
[h] *Graduate School of Advanced Technology and Science, Tokushima University, Tokushima, 770-8506, Japan*
[i] *Nuclear Science Division, Lawrence Berkeley National Laboratory, Berkeley, CA, 94720, USA*
[j] *Department of Physics and Astronomy, University of Hawaii at Manoa, Honolulu, HI, 96822, USA*
[k] *Massachusetts Institute of Technology, Cambridge, 02139, MA, USA*
[l] *Boston University, Boston, MA, 02215, USA*
[m] *Department of Physics and Astronomy, University of Tennessee, Knoxville, TN, 37996, USA*
[n] *Triangle Universities Nuclear Laboratory, Durham, NC, 27708, USA*
[o] *The University of North Carolina at Chapel Hill, Chapel Hill, NC, 27599, USA*
[p] *North Carolina Central University, Durham, NC, 27701, USA*
[q] *Physics Department at Duke University, Durham, NC, 27705, USA*
[r] *Center for Experimental Nuclear Physics and Astrophysics, University of Washington, Seattle, WA, 98195, USA*
[s] *Nikhef and the University of Amsterdam, Science Park, Amsterdam, the Netherlands*
[t] *Center for Neutrino Physics, Virginia Polytechnic Institute and State University, Blacksburg, VA, 24061, USA*

Abstract

We report the results of a search for MeV-scale astrophysical neutrinos in KamLAND presented as an excess in the number of coincident neutrino interactions associated with the publicly available high-energy neutrino datasets from the IceCube Neutrino Observatory. We find no statistically significant excess in the number of observed low-energy electron antineutrinos in KamLAND, given a coincidence time window of ±500 s, ±1,000 s, ±3,600 s, and ±10,000 s around each of the IceCube neutrinos. We use this observation to present limits from 1.8 MeV to 100 MeV on the electron antineutrino fluence, assuming a mono-energetic flux. We then compare the results to several astrophysical measurements performed by IceCube and place a limit at the 90% confidence level on the electron antineutrino isotropic thermal luminosity from the TXS 0506+056 blazar.

Keywords: neutrinos, astrophysical neutrinos

1. Introduction

Astrophysical neutrinos are capable of delivering unprecedented information about the most cataclysmic events in the Universe. Since neutrinos only interact weakly with matter and are not deflected by galac-

tic/intergalactic magnetic fields, they point back to their production source and carry information relating to the in situ physical conditions of some of nature's most extreme environments. The remarkable discovery of the diffuse astrophysical neutrino flux in 2013 [1, 2, 3] by the cubic-kilometer IceCube Neutrino Observatory issued neutrinos into the toolkit for extragalactic multimessenger astronomy and realized the potential of finding an extragalactic neutrino point source in the near future. A breakthrough arrived on 22 September 2017, when IceCube detected a high-energy muon neutrino (IceCube-170922A) in coincidence with, and in the direction of, a flaring gamma-ray blazar (TXS 0506+056) [4]. The significance of this observation, when including the antecedent neutrino flux originating from the direction of TXS 0506+056 in conjunction with data collected by Large Area Telescope (LAT) on the Fermi Gamma-ray Space Telescope [5] and the Major Atmospheric Gamma Imaging Cherenkov (MAGIC) telescopes [6, 7], was found to be approximately 3.5σ [4]. This observation provided the most compelling evidence supporting the long-suspected theory that jetted active galactic nuclei (AGN) contribute to highest energy ($\gtrsim$100 TeV) extragalactic neutrino background [8, 9, 10]. The diffuse astrophysical neutrino spectrum, however, appears to disfavour a single-zone model [11, 12], in which the high-energy neutrinos are produced in a single emission region. The most recent studies have reported a 2.9σ neutrino excess at the coordinates of NGC 1068 [13], a radio quiet AGN; a 2.6σ excess compatible with neutrino production in the cores of AGNs [14]; and the association of two radio-emitting tidal disruption events, AT2019dsg and AT2019fdr, with a $\sim$0.2 PeV and $\sim$0.08 PeV neutrino [15, 16], respectively.

Following these recent scientific advancements, an international effort has emerged to develop of the next generation of high-energy astrophysical neutrino observatories: KM3NeT-ORCA and KM3NeT-ARCA [17] off the coast of France and Scicily; Baikal-GVD [18] in Siberia; IceCube-Gen2 [19] in Antarctica; and the Pacific Ocean Neutrino Experiment (P-ONE) [20] off the west coast of Vancouver Island in Canada. While evidence mounts towards the determination of the source(s) of the high-energy astrophysical neutrinos the correlation between MeV and TeV-to-PeV neutrino production remains unclear. Many astrophysical objects exhibit spectra characteristic of an ultra-relativistic collimated jet formation that can give rise to a secondary neutrino beam. Neutrinos may also be produced in the accretion disk, the resulting disk corona, and/or through the molecular wind/outflow from these objects. In any case, the models involve significant astrophysical uncertainties [21, 22, 23], and motivate experimental searches at lower energies. The Super-Kamiokande experiment has recently published the null observation of a 225 kiloton-years search for the GeV astrophysical neutrino counterpart [24], and the null observation of a 22-year GeV to several TeV search specifically looking for a neutrino excess in the direction of TXS 0506+056 [25].

In this analysis, we present a search for time-correlated MeV electron antineutrino ($\bar{\nu}_e$) events in the Kamioka Liquid Scintillator Antineutrino Detector (KamLAND) associated with several publicly available high-energy neutrino datasets from IceCube. We include data spanning from 9 October 2010 through to 12 June 2021. We use KamLAND electron antineutrinos with energies ranging from 1.8 MeV$< E_{\bar{\nu}_e} <$100 MeV, thus making this the lowest energy astrophysical coincident neutrino search associated with IceCube to date. Observing the low-energy counterpart of the astrophysical neutrino flux would not only help with source identification but also with understanding the neutrino energy spectrum and production mechanism.

2. KamLAND detector

KamLAND is a kiloton-class liquid scintillator neutrino detector situated 1 km below the surface of Mt. Ikenoyama in Kamioka, Japan. KamLAND is separated into an inner and outer detector, demarcated by an 18 m spherical stainless steel tank. The inner detector was primarily optimized for MeV electron antineutrino ($\bar{\nu}_e$) detection [26, 27, 28]. It contains a 13 m diameter transparent balloon holding approximately 1,200 m^3 of ultrapure liquid scintillator. Scintillation light is observed by 1,325 17-inch photomultipliers (PMT) and 554 20-inch PMTs suspended in a buffer-oil solution. The PMTs point radially inwards into the inner detector providing approximately 34% photocathode coverage. This analysis considers the fiducial volume of the detector to be the innermost 12 m diameter region of the inner detector. The outer detector contains 3.2 kton of pure water that acts as a cosmic-ray muon veto and passive shield against radioactivity originating in the surrounding material. The full KamLAND detector is synchronized to an

external Global Positioning System receiver placed outside the entrance to the Kamioka mine, providing a global time uncertainty of less than 100 μs.

From August 2011 up to October 2015, a transparent teardrop-shaped, 3.0 m-diameter inner balloon containing approximately 350 kg of enriched ^{136}Xe was installed into the central region of the inner detector as a part of KamLAND-Zen 400 experiment [29]. This was replaced with a larger inner balloon containing approximately 700 kg of enriched ^{136}Xe in April 2018 for the KamLAND-Zen 800 experiment [30, 31].

3. Electron antineutrino selection in KamLAND and background estimation

We consider the KamLAND events triggered by the inverse beta decay (IBD) interaction, where a $\bar{\nu}_e$ interacts weakly with a proton producing a positron and neutron in the final state ($\bar{\nu}_e + p \rightarrow e^+ + n$). In this interaction, the positron quickly deposits its kinetic energy into the scintillator and annihilates with an electron near the primary interaction vertex, creating a *prompt* signal. The neutron thermalizes via elastic scatters before capturing on a proton (carbon-12) atom producing a deuteron (carbon-13) and a 2.2 MeV (4.5 MeV) gamma ray. The thermal diffusion of the neutron has a mean capture time of $207.5 \pm 2.8\,\mu s$ [32] and the emission of the gamma ray is observed as a *delayed* signal. The time and space correlation between the successive delayed coincidence (DC) signals allows for efficient background suppression, enabling a high-efficiency detection of IBD interactions. Specifically, we require the delayed interaction vertex to be located within 200 cm of the prompt signal, and the time difference between the delayed and prompt signal to be less than 1000 μs. The interaction vertex resolution in KamLAND can be approximated as $12\,\mathrm{cm}/\sqrt{E_{\bar{\nu}_e}(\mathrm{MeV})}$ [26]. Since the angular distribution of the positron is nearly isotropic and the scintillation light emission is also isotropic, KamLAND is unable to reconstruct the direction of the incident $\bar{\nu}_e$.

The IBD interaction has a kinematic low-energy neutrino threshold of $E_{\bar{\nu}_e} = 1.806$ MeV. We can relate $E_{\bar{\nu}_e}$ to the measured prompt energy, E_p, via $E_{\bar{\nu}_e} \approx E_p + 0.78\,\mathrm{MeV} + T_n$, where T_n is neutron kinetic energy. The thermalization of the neutron is also contained in the prompt signal, however it is sufficiently quenched that it can be ignored in the energy range of this analysis. The delayed energy is selected to be between $1.8\,\mathrm{MeV} \leq E_d \leq 2.6\,\mathrm{MeV}$ or $4.4\,\mathrm{MeV} \leq E_d \leq 5.6\,\mathrm{MeV}$ and the prompt energy is selected to be between $0.9\,\mathrm{MeV} \leq E_p \leq 93\,\mathrm{MeV}$. The IBD selection criteria also includes a likelihood-based series of cuts capable of further reducing the background, described in Ref. [26]. This accounts for the accidental coincidence events, detector refurbishment [33], inner balloon installation [30, 31], and the status of the Japanese nuclear reactors. We approximate the energy resolution of KamLAND as $6.4\%/\sqrt{E_{\bar{\nu}_e}(\mathrm{MeV})}$ [26].

The KamLAND IBD data used in this analysis is separated into four time periods. Period I refers to the data collected prior to the installation of the KamLAND-Zen 400 inner balloon on 12 October 2011. This period includes an additional cut on the prompt energy, such that events with $E_p < 7.5$ MeV are rejected in order to reduce the reactor neutrino background. Since all Japanese nuclear reactors were shut down in March 2011, due to the Great East Japan Earthquake, subsequent periods do not include this cut. Period II refers to the data taking period in which the KamLAND-Zen 400 inner balloon was installed in the detector (12 October 2011 to 24 October 2015). Here, we include an additional geometric cut on the delayed event around the inner balloon and support structure to reduce backgrounds introduced by the additional material. The cut removes events in which the delayed signal occurs within the central spherical 2.5 m radius region, extending to the top of the detector in a 2.5 m radius cylinder. We account for the reduction in fiducial volume due to this cut in the detection efficiency rather than the number of target nuclei. Period III spans the time between the extraction of the KamLAND-Zen 400 inner balloon (24 October 2015) and 16 April 2018, the start of KamLAND-Zen 800. During this period, we do not include the 2.5 m radius geometric cut. The final period, Period IV, includes all data from the introduction of the KamLAND-Zen 800 inner balloon (16 April 2018) onwards. Here, we also include the same geometric cut described for Period II. The realtime and livetime, along with the livetime efficiency, ϵ_{live}, for each period are shown in the leftmost columns of Table 1.

KamLAND data is recorded in runs, which tend to span approximately one day. We impose quality checks on each run to ensure that the detector was in suitable operating condition and not taking data during calibration. The final IBD event sample was found to contain 341 IBD events. We consider all IBD interactions in the background calculation, since a possible correlated neutrino with an IceCube event would

provide a negligible contribution to the sample. Table 1 shows the number of IBD events observed in each period during the detector livetime.

In Period I, the IBD sample is dominated by atmospheric neutrinos. There is also a significant contribution arising from long-lived spallation products and fast neutrons from cosmic-ray muons [34]. While these are also the dominant background above $E_p > 7.5\,\text{MeV}$ in Period II - IV, below this energy neutrinos originating from the small number of operational Japanese nuclear reactor power plants dominate the IBD sample. At energies below $\sim$3.4 MeV, there is also a contribution from radiogenic neutrinos originating from the decay of ^{40}K, ^{232}Th, and ^{238}U within the Earth. The IBD sample also includes a small number of accidental DC signals induced by the decay of radioactive impurities, additional radioactive products from cosmic-ray muon spallation [32, 35], and the alpha-induced ^{13}C(α,n)^{16}O reaction in the liquid scintillator.

Table 1: The period-specific data used in this analysis, assuming a time window of $\pm$500 s. Given the total number of expected background events in each period along with the null observation of a coincident event, the last column shows the corresponding Feldman-Cousins 90% C.L. upper limit on the number of observed signal neutrinos.

	Realtime [days]	Livetime [days]	ϵ_{live} [%]	IBD Counts	HE Events Counts	Total Window [h]	Total Bkg. Counts	Total Sig. Counts	N_{90} Counts
Period I	393.4	244.7	62.2	3	4	1.1	5.7×10^{-4}	0	2.43
Period II	1471.9	1370.4	93.1	148	22	6.1	2.7×10^{-2}	0	2.40
Period III	561.0	482.0	85.9	58	14	3.9	2.0×10^{-2}	0	2.41
Period IV	1152.7	1094.0	94.9	132	62	17.2	8.7×10^{-2}	0	2.34
Total	3579.0	3191.1	89.2	341	102	28.3	13.4×10^{-2}	0	2.30

4. IceCube high-energy neutrino sample

Historical IceCube neutrino events that met the criteria of the Extremely High Energy (EHE) and High Energy Starting Event (HESE) IceCube filters were taken from a publicly available data release[1]. The first of these events was on 9 October 2010. The historical EHE filter contained twenty four track-like (muon neutrino) events originating from the Northern Hemisphere with neutrino energies greater than several hundred TeV. The historical HESE filter contained sixteen track-like events whose interaction vertices originated within the instrumented volume of IceCube, five of which have since been retracted due to poor angular reconstruction. Since the HESE events start within the instrumented volume, this filter is also capable of accepting events that originate from the Southern Hemisphere. These two filters were subsequently added to the realtime Astrophysical Multimessenger Observatory Network (AMON) in early 2016. Depending on the signal, AMON distributes alerts in realtime for follow-up observations via the Gamma-ray Coordinates Network (GCN). In total, there have been nine EHE[2] and eighteen HESE[3] realtime alerts issued. A single event was reported on both the AMON EHE and HESE system.

The EHE and HESE realtime alerts continued until 2019 May, when a new classification scheme referred to as "Gold" and "Bronze"[4] was introduced. The set of Gold events is expected have an astrophysical purity greater than 50%, whereas the purity of the Bronze sample is expected to be greater than 30%. Since this change, there have been tweenty-two Gold and thirty-one Bronze alerts issued prior to 12 June 2021, the end date of this analysis. A separate realtime alert classification also exists for the high-energy electron (anti)neutrino and neutral current events, known as the Cascade filter.[5] This filter contains three events, all of which were issued in 2021, and is expected to have an astrophysical purity $>85\%$.

[1] https://icecube.wisc.edu/data-releases/2018/07/
[2] https://gcn.gsfc.nasa.gov/amon_ehe_events.html
[3] https://gcn.gsfc.nasa.gov/amon_hese_events.html
[4] https://gcn.gsfc.nasa.gov/amon_icecube_gold_bronze_events.html
[5] https://gcn.gsfc.nasa.gov/amon_icecube_cascade_events.html

The IceCube-170922A event, discussed in Sec. 1, is expected to have originated from the flaring gamma-ray blazar, TXS 0506+056. The redshift was measured using Gran Telescopio Canarias and found to have a redshift of $z = 0.3365 \pm 0.0010$, corresponding to the luminosity distance of $d = 1.75\,\mathrm{Gpc}$ [36]. The IceCube-170922A event triggered the EHE filter and had a reconstructed energy of approximately 290 TeV, with a 90% confidence level (C.L.) lower limit of 183 TeV. It was reported on AMON with a follow-up campaign through the GCN from electromagnetic observatories.

Finally, an event was recently found to have a reconstructed visible energy of 6.05 ± 0.72 PeV, consistent with a $\bar{\nu}_e$ interacting via the Glashow resonance [37]. The evidence of the Glashow resonance indicates the presence of $\bar{\nu}_e$s in the astrophysical flux. This event had its own data-release.[6]

Of the 118 IceCube events described above, 102 arrived during the livetimes considered in this analysis.

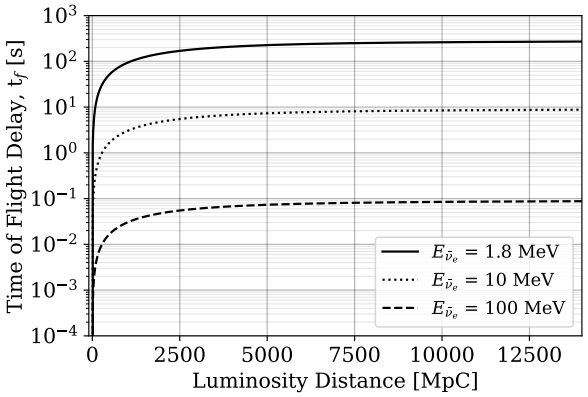

Figure 1: A conservative estimate of the time of flight delay of a massive neutrino with an energy of 1.8 MeV (solid), 10 MeV (dotted), and 100 MeV (dashed), relative to the speed of light. The time of flight delay of a 1.8 MeV neutrino originating at the location of TXS 0506+056 is determined to be less than 138 s.

5. Correlated event search

With no conclusive single source of astrophysical neutrinos or theoretical production mechanism to link the high-energy to the low-energy neutrino flux, we attempt to reduce model-dependency by selecting various time windows to search for an excess number of coincident events. We define a coincidence search time window around each of the high-energy neutrinos in IceCube, t_{HE}, such that:

$$t_{HE} - t_p < t_{IBD} < t_{HE} + t_p, \tag{1}$$

where t_{IBD} is the IBD prompt signal global timestamp and t_p represents a predefined window size that is sufficiently large to cover the low-energy neutrino time of flight delay and model-dependency.

The time of flight delay relative to the speed of light for a neutrino with redshift z, mass m_ν, and energy E_ν, can be calculated through:

$$t_f = \frac{1}{2H_0}\frac{m_\nu^2}{E_\nu^2}\int_0^z \frac{1}{(1+z)^2\sqrt{\Omega_\Lambda + \Omega_M(1+z)^3}}, \tag{2}$$

where we assume base-ΛCDM cosmology parameters from Ref. [38]: Hubble constant $H_0 = 67.4\,\mathrm{km\,s^{-1}\,Mpc^{-1}}$; matter density parameter $\Omega_M = 0.315$; and dark matter density parameter $\Omega_\Lambda = 0.685$. The mass of the electron antineutrino is conservatively set to $\mathrm{m}_\nu = 0.087\,\mathrm{eV}$, that is, the approximate 90% C.L. upper limit on the most massive neutrino mass eignenstate, given a normal mass hierarchy with mass squared splittings

[6] https://icecube.wisc.edu/data-releases/2021/03/icecube-data-for-the-first-glashow-resonance-candidate/

from Ref. [39], and using the sum of the neutrino masses to be $\sum m_\nu = 0.12\,\text{eV}$ [38]. The time of flight delay, calculated from Eq. 2, is shown in Fig. 1 for several neutrino energies. We find that even for the most distant source, the time of flight for a 1.8 MeV neutrino is less than 270 s.

Given the maximum expected time of flight delay, we choose to define the minimal time window used in this analysis to be t_p = (a) 500 s. This is a commonly adopted time window range used for similar analyses that search for correlated neutrinos with gravitational waves [40, 41, 42] and gamma-ray bursts (GRB) [41, 43, 44]. Since there are some cosmological events that span more than 1,000 s, such as the longest duration GRBs, we also use several more conservative time windows of t_p = (b) 1,000 s, (c) 3,600 s, and (d) 10,000 s. This is also a common strategy for coincident searches with large uncertainties on the progenitors model [44]. If any of the time windows extend into a new KamLAND run or over a short period of detector deadtime, we ensure that at least 90% of the total time window is covered by KamLAND livetime.

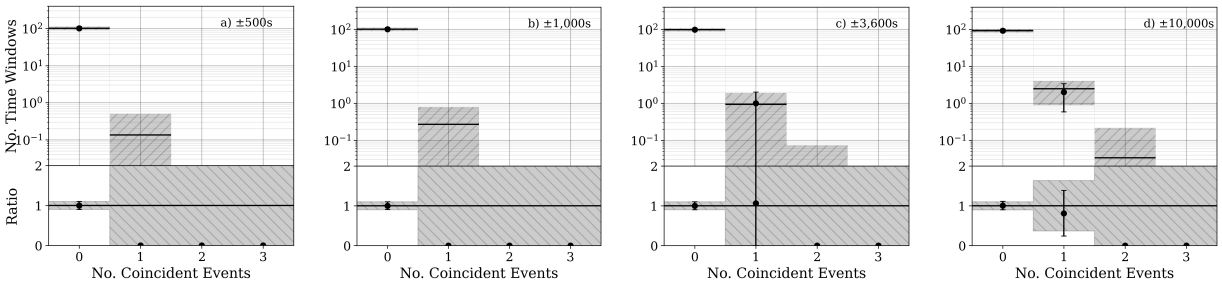

Figure 2: The number of observed signal candidates are shown as black data points with statistical uncertainties for each of the four predefined time windows: (a) ±500s, (b) ±1,000 s, (c) ±3,600 s, and (d) ±10,000 s. The black horizontal lines represent the expected number of events given the Poissonian background reported in Table 1 along with the hatched area representing the statistical uncertainty. The ratio of the number of observed signal candidates to the background expectation is shown in the lower subplots.

6. Results

The number of observed signal candidates in the predefined time windows, compared to the Poisson-fluctuated IBD background expectation, is shown in Fig. 2. No significant observation above the expected background is observed in any time window. Zero coincident events were observed using time windows (a) and (b). A single IBD event was observed in coincidence with a high-energy IceCube event (IceCube run number 132229 and event number 66688965) in time window (c). Time window (d) observed a second coincident event (IceCube run number 134817 and event number 29175858). These observations, however, are compatible with the background expectation for time windows (c) and (d): 0.94 and 2.51 events, respectively. The first coincident event occurred on 21 February 2019 (Period IV), at 07:51:55.569 (UTC). The IceCube track-like neutrino[7] was categorized as a Gold event and reported to have an energy of approximately 56 TeV. The KamLAND IBD interaction occurred 2024 s prior to the IceCube neutrino and had an energy of 5.2 ± 0.1 MeV. The second coincident event occurred on 21 December 2020 (Period IV) at 15:16:24.736 (UTC). The IceCube event was also track-like, [8] categorized as a Gold event, and had a measured energy of approximately 175 TeV. The KamLAND neutrino had a reconstructed energy of 3.1 ± 0.1 MeV and arrived 9571.3 s after the IceCube neutrino.

The closest IBD timestamp to IceCube-170922A arrived 222,048 s (2.57 days) prior to the IceCube event. The Poisson probability of observing a single coincident event arriving within this time window is approximately 23%. The high-energy gamma radiation observed by MAGIC ($E_\gamma > 90$ GeV), H.E.S.S. ($E_\gamma > 175$ GeV),

[7] https://gcn.gsfc.nasa.gov/gcn3/23918.gcn3
[8] https://gcn.gsfc.nasa.gov/gcn3/29102.gcn3

and VERITAS ($E_\gamma > 175$ GeV) found that the TXS 0506+056 blazar was in a high-emission state for ∼12 days after the observation of IceCube-170922A. In this time span, KamLAND observed two IBD events occurring 8.73 and 9.35 days after IceCube-170922A. These two events had a prompt energy of $E_{\bar{\nu}_e} = 2.4 \pm 0.1$ and 3.1 ± 0.1, respectively. This observation is also consistent with the IBD background expectation, and the Poisson probability of observing two events within this time window is 21%.

In the absence of a signal, we present the 90% C.L. upper limit on the number of observed signal neutrinos, N_{90}, for the ±500 s time window using the Feldman-Cousins method [45]. The period-dependent values are listed in the right-most column of Table 1. The 90% C.L. upper limit on the $\bar{\nu}_e$ fluence for each high-energy neutrino in period k is then given by:

$$F_{90}^k = \frac{N_{90}^k}{N_T \int \sigma(E_{\bar{\nu}_e}) \lambda(E_{\bar{\nu}_e}) \epsilon_s^k(E_{\bar{\nu}_e}) dE_{\bar{\nu}_e}}, \tag{3}$$

where the integral is performed over the energy range of this analysis, $N_T = 5.98 \times 10^{31}$ is the number of target protons in fiducial volume, $\sigma(E_{\bar{\nu}_e})$ is the IBD cross-section [46], $\lambda(E_{\bar{\nu}_e})$ is the normalized $\bar{\nu}_e$ energy spectrum, and ϵ_s^k is the IBD detection efficiency found in Fig. 3 (left). Prior to making an assumption on $\lambda(E_{\bar{\nu}_e})$, we compute the equivalent fluence Greene's function using a mono-energetic neutrino flux by replacing $\lambda(E_{\bar{\nu}_e})$ with a delta function:

$$\Psi_{90}^k(E_{\bar{\nu}_e}) = \frac{N_{90}^k}{N_T \int \sigma(E'_{\bar{\nu}_e}) \delta(E_{\bar{\nu}_e} - E'_{\bar{\nu}_e}) \epsilon_s^k(E'_{\bar{\nu}_e}) dE'_{\bar{\nu}_e}}. \tag{4}$$

Fig. 3 (right) shows the 90% C.L. upper limit on the mono-energetic $\bar{\nu}_e$ fluence, for each of the four KamLAND periods. The curves shown here are also a close approximation of the experimental sensitivity for each period. We note that the presented limits modestly change when using the more conservative time windows. For Periods I - III the limits are found to decrease by less than 10% for all time windows. The observation a single coincident event using time window (c) and two events using time window (d), increase the Period IV limit by 59.4% and 81.6%, respectively.

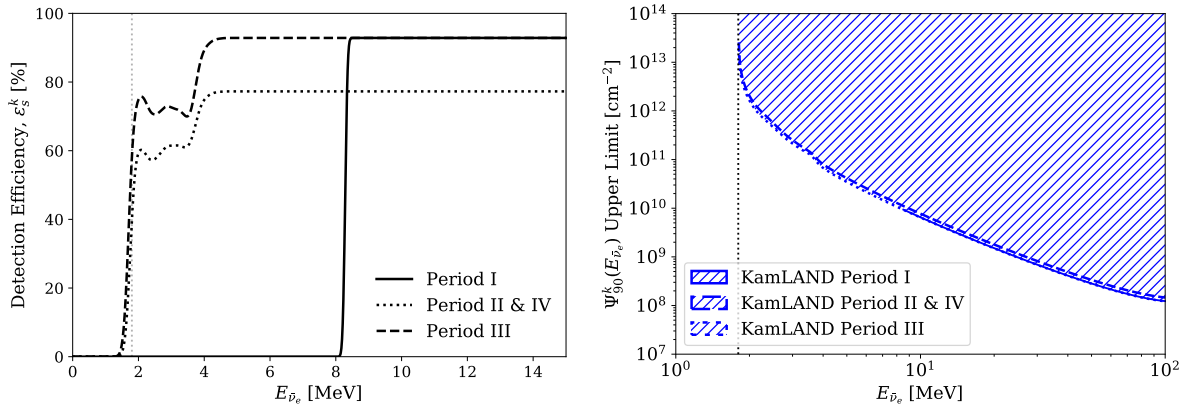

Figure 3: Left: The IBD detection efficiencies as a function of reconstructed $E_{\bar{\nu}_e}$ for each KamLAND period. Above 5 MeV, the detection efficiencies converge to approximately 92.9% and 77.4% for Periods I & III and II & IV, respectively. The structure below 4 MeV is primarily due to the likelihood-based selection criteria. The non-zero detection efficiency below the low-energy IBD threshold arises from the finite energy resolution in KamLAND. Right: The 90% C.L. upper limit on the mono-energetic $\bar{\nu}_e$ fluence, for energies between $E_{\bar{\nu}_e} = 1.8$ MeV and 100 MeV. The results of Periods II & IV are within the line width of each other. In both figures, a vertical dotted line is shown at the IBD threshold.

The neutrino flux is often modeled as an isotropic unbroken power-law spectrum [47] defined by a

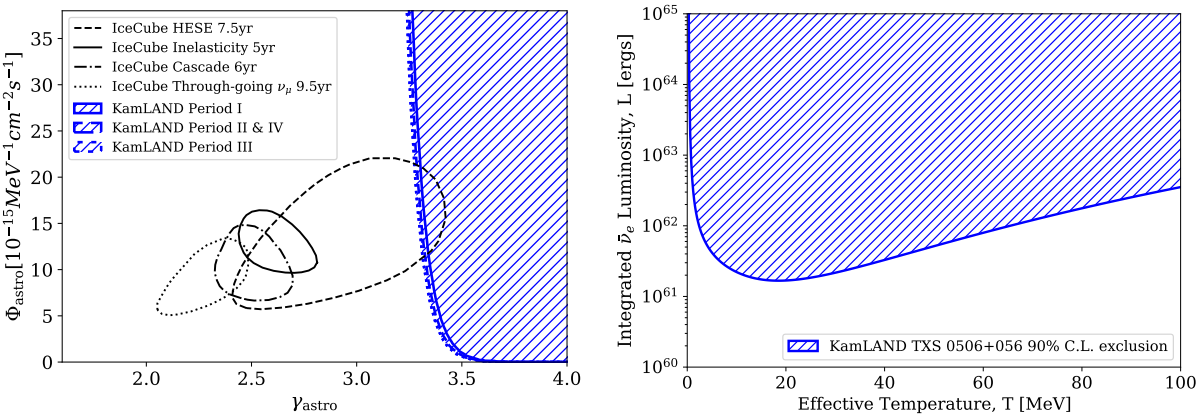

Figure 4: Left: The excluded astrophysical flux parameters, $\Phi_{\rm astro}$ and $\gamma_{\rm astro}$, at the 90% C.L. from KamLAND, assuming an unbroken power-law energy spectrum. Also shown is the IceCube's 95.4% confidence regions from the 7.5yr HESE sample [48], the 5yr inelasticity measurement [49], the 6yr cascade sample [3], the 9.5yr Northern track sample preliminary results [50]. The normalization constant is presented per neutrino species, integrated over the full sky. Right: The 90% C.L. excluded $\bar{\nu}_e$ luminosity and effective source temperature, assuming a Fermi-Dirac energy distribution at the distance of the TXS 0506+056 blazar.

normalization constant at 100 TeV, $\Phi_{\rm astro}$, and spectral index, $\gamma_{\rm astro}$:

$$\lambda_{PL}(E_{\bar{\nu}_e}, \Phi_{\rm astro}, \gamma_{\rm astro}) = \Phi_{\rm astro}\left(\frac{E_{\bar{\nu}_e}}{100\,\text{TeV}}\right)^{-\gamma_{\rm astro}}. \tag{5}$$

This is the model that IceCube primarily employs to fit their high-energy neutrino datasets [48, 49, 3, 50]. We can extrapolate our null observation limits to higher energies to compare with the IceCube results. Using the derived 90% C.L. upper limit on the number of observed signal neutrinos in period k, the excluded region in terms of the parameter space described in Eq. 5, is calculated as:

$$N_{90}^k = N_T \int \epsilon_s^k(E_{\bar{\nu}_e})\sigma(E_{\bar{\nu}_e})\lambda(E_{\bar{\nu}_e})dE_{\bar{\nu}_e}, \tag{6}$$

where we set $\lambda(E_{\bar{\nu}_e}) = \lambda_{PL}(E_{\bar{\nu}_e}, \Phi_{\rm astro}, \gamma_{\rm astro})$. Fig. 4 (Left) shows the excluded part of the unbroken power-law spectrum for a single astrophysical neutrino, compared to the allowed 95.4% confidence region per neutrino species from IceCube. The slight tension between the different IceCube measurements could be an indication that a simple unbroken power-law fit is not sufficient to describe the astrophysical neutrino flux spectrum. As in the case of the astrophysical cosmic rays, it could be the case that there is a break or low-enegy cut-off in the spectrum below the high-energy domain of IceCube and the low energies observed in KamLAND.

The high-temperature environment of the flaring TXS 0506+056 blazar may also emit MeV-scale thermal neutrinos. The thermal emission can be modeled as a Fermi-Dirac distribution at an effective temperature, T, with zero chemical potential:

$$\Phi_{FD}(E_{\bar{\nu}_e}, T) = \frac{1}{T^3 f_2}\frac{E_{\bar{\nu}_e}^2}{e^{(E_{\bar{\nu}_e}/T)}+1}, \quad f_n = \int_0^\infty \frac{x^n}{e^x+1}dx. \tag{7}$$

The at-Earth flux, given the redshift and luminosity distance to TXS 0506+056, is calculated through:

$$\lambda_{FD}(E_{\bar{\nu}_e}, T, L) = \frac{1+z}{4\pi d^4}\frac{L}{\langle E\rangle}\Phi_{FD}((1+z)E_{\bar{\nu}_e}, T), \tag{8}$$

where L is the isotropic source $\bar{\nu}_e$ luminosity. As in Ref. [40], we relate the mean $\bar{\nu}_e$ energy to the ef-

fective temperature through $\langle E \rangle = 3.15T$. We now set $\lambda(E_\nu) = \lambda_{FD}(E_{\bar{\nu}_e}, T, L)$ in Eq. 6 to compute the 90% C.L. limits on the integrated $\bar{\nu}_e$ luminosity as a function of source effective temperature. Fig. 4 (right) shows the excluded region for TXS 0506+056 based on the null observation. The presented limit assumes an isotropic thermal neutrino emission. Due to the large distance to the TXS 0506+056 blazar, the limits are approximately nine orders of magnitude higher than the $\bar{\nu}_e$ luminosity/temperature of supernova SN1987A [51, 52, 53].

7. Conclusion

In this analysis, we performed a search for low-energy electron antineutrinos in KamLAND correlated with the publicly available high-energy neutrino datasets from the IceCube Neutrino Observatory. The analysis examined over ninety-five high-energy neutrino events in IceCube for correlations with 341 low-energy KamLAND neutrinos, spanning from October 2010 to June 2021. No significant excess above the expected background was observed using a coincident time window of ±500s, ±1,000 s, ±3,600 s and ±10,000 s. Given the null observation, the 90% C.L. upper limit assuming a mono-energetic neutrino flux was presented. A comparison to the measured IceCube astrophysical flux, assuming an unbroken power-law energy spectrum, was also performed. Finally, using the redshift to the TXS 0506+056 blazar, we also presented limits on the isotropic thermal MeV-scale neutrino emission assuming a Fermi-Dirac energy spectrum.

8. Acknowledgments

The KamLAND experiment is supported by JSPS KAKENHI Grants 19H05803; the World Premier International Research Center Initiative (WPI Initiative), MEXT, Japan; Netherlands Organization for Scientific Research (NWO); and under the U.S. Department of Energy (DOE) Contract No. DE-AC02-05CH11231, the National Science Foundation (NSF) No. NSF-1806440, NSF-2012964, the Heising-Simons Foundation, as well as other DOE and NSF grants to individual institutions. The Kamioka Mining and Smelting Company has provided services for activities in the mine. We acknowledge the support of NII for SINET4.

References

[1] M. Aartsen, et al., Evidence for high-energy extraterrestrial neutrinos at the IceCube detector, Science 342 (6161) (2013) 1242856. arXiv:arXiv:1311.5238v2.
[2] M. Aartsen, et al., Atmospheric and astrophysical neutrinos above 1 TeV interacting in IceCube, Physical Review D 91 (2) (2015) 022001.
[3] M. Aartsen, et al., Characteristics of the diffuse astrophysical electron and tau neutrino flux with six years of IceCube high energy cascade data, Physical review letters 125 (12) (2020) 121104.
[4] M. Aartsen, et al., Neutrino emission from the direction of the blazar TXS 0506+056 prior to the IceCube-170922A alert, Science 361 (6398) (2018) 147–151. doi:10.1126/science.aat2890.
URL http://dx.doi.org/10.1126/science.aat2890
[5] Y. T. Tanaka, S. Buson, D. Kocevski, Fermi-LAT detection of increased gamma-ray activity of TXS 0506+ 056, located inside the IceCube-170922A error region., The Astronomer's Telegram 10791 (2017) 1.
[6] J. Aleksić, et al., Performance of the MAGIC stereo system obtained with Crab Nebula data, Astroparticle Physics 35 (7) (2012) 435–448.
[7] R. Mirzoyan, First-time detection of VHE gamma rays by MAGIC from a direction consistent with the recent EHE neutrino event IceCube-170922A, The Astronomer's Telegram 10817 (2017) 1.
[8] F. Halzen, D. Hooper, High energy neutrinos from the TeV Blazar 1ES 1959+ 650, Astroparticle Physics 23 (6) (2005) 537–542.
[9] S. Adrián-Martínez, et al., Search for neutrino emission from gamma-ray flaring blazars with the ANTARES telescope, Astroparticle Physics 36 (1) (2012) 204–210.
[10] M. Kadler, et al., Coincidence of a high-fluence blazar outburst with a PeV-energy neutrino event, Nature Physics 12 (8) (2016) 807–814.
[11] A. Keivani, et al., A multimessenger picture of the flaring blazar TXS 0506+ 056: implications for high-energy neutrino emission and cosmic-ray acceleration, The Astrophysical Journal 864 (1) (2018) 84.
[12] M. Aartsen, et al., The contribution of FERMI-2LAC blazars to diffuse TeV–PeV neutrino flux, The Astrophysical Journal 835 (1) (2017) 45.

[13] M. Aartsen, M. Ackermann, J. Adams, J. Aguilar, M. Ahlers, M. Ahrens, C. Alispach, K. Andeen, T. Anderson, I. Ansseau, et al., Time-integrated neutrino source searches with 10 years of IceCube data, Physical review letters 124 (5) (2020) 051103.
[14] R. Abbasi, et al., A search for neutrino emission from cores of Active Galactic Nuclei, arXiv preprint arXiv:2111.10169 (2021).
[15] R. Stein, et al., A tidal disruption event coincident with a high-energy neutrino, Nature Astronomy 5 (5) (2021) 510–518.
[16] S. Reusch, et al., The candidate tidal disruption event AT2019fdr coincident with a high-energy neutrino, arXiv preprint arXiv:2111.09390 (2021).
[17] S. Adrian-Martinez, et al., Letter of intent for KM3NeT 2.0, Journal of Physics G: Nuclear and Particle Physics 43 (8) (2016) 084001.
[18] B.-G. Collaboration, et al., Baikal-GVD: status and prospects (2018).
[19] M. Aartsen, et al., IceCube-Gen2: the window to the extreme universe, Journal of Physics G: Nuclear and Particle Physics 48 (6) (2021) 060501.
[20] M. Agostini, et al., The Pacific Ocean Neutrino Experiment, Nature Astronomy 4 (10) (2020) 913–915.
[21] P. Mészáros, Astrophysical sources of high-energy neutrinos in the IceCube era, Annual Review of Nuclear and Particle Science 67 (2017) 45–67.
[22] K. Murase, Active galactic nuclei as high-energy neutrino sources, in: neutrino astronomy: current status, future prospects, World Scientific, 2017, pp. 15–31.
[23] J. G. Learned, K. Mannheim, High-energy neutrino astrophysics, Annual Review of Nuclear and Particle Science 50 (1) (2000) 679–749.
[24] K. Abe, et al., Search for an excess of events in the Super-Kamiokande detector in the directions of the astrophysical neutrinos reported by the IceCube Collaboration, The Astrophysical Journal 850 (2) (2017) 166.
[25] K. Hagiwara, et al., Search for astronomical neutrinos from blazar TXS 0506+ 056 in Super-Kamiokande, The Astrophysical Journal Letters 887 (1) (2019) L6.
[26] A. Gando, et al., Reactor on-off antineutrino measurement with KamLAND, Phys. Rev. D 88 (2013) 033001. doi:10.1103/PhysRevD.88.033001.
URL https://link.aps.org/doi/10.1103/PhysRevD.88.033001
[27] T. Araki, et al., Experimental investigation of geologically produced antineutrinos with KamLAND, Nature 436 (7050) (2005) 499–503. doi:10.1038/nature03980.
[28] S. Abe, et al., Precision measurement of neutrino oscillation parameters with KamLAND, Physical Review Letters 100 (22) (2008) 221803. doi:10.1103/PhysRevLett.100.221803.
[29] A. Gando, et al., Search for Majorana neutrinos near the inverted mass hierarchy region with KamLAND-Zen, Physical Review Letters 117 (8) (2016) 082503. doi:10.1103/PhysRevLett.117.082503.
[30] Y. Gando, et al., First results of KamLAND-Zen 800, in: Journal of Physics: Conference Series, Vol. 1468, IOP Publishing, 2020, p. 012142. doi:10.1088/1742-6596/1468/1/012142.
[31] Y. Gando, et al., The nylon balloon for xenon loaded liquid scintillator in KamLAND-Zen 800 neutrinoless double-beta decay search experiment, JINST 16 (08) (2021) P08023. doi:10.1088/1748-0221/16/08/p08023.
URL https://doi.org/10.1088/1748-0221/16/08/p08023
[32] S. Abe, et al., Production of radioactive isotopes through cosmic muon spallation in KamLAND, Phys. Rev. C 81 (2010) 025807. doi:10.1103/PhysRevC.81.025807.
URL https://link.aps.org/doi/10.1103/PhysRevC.81.025807
[33] H. Ozaki, J. Shirai, Refurbishment of KamLAND outer detector, PoS, ICHEP2016 1161 (2017). doi:10.22323/1.282.1161.
[34] A. Gando, et al., Search for extraterrestrial antineutrino sources with the KamLAND detector, The Astrophysical Journal 745 (2) (2012) 193.
[35] S. Abe, et al., Limits on astrophysical antineutrinos with the kamland experiment, The Astrophysical Journal 925 (1) (2022) 14.
[36] S. Paiano, R. Falomo, A. Treves, R. Scarpa, The Redshift of the BL Lac Object TXS 0506+056, The Astrophysical Journal 854 (2) (Feb 2018). doi:10.3847/2041-8213/aaad5e.
URL http://dx.doi.org/10.3847/2041-8213/aaad5e
[37] M. Aartsen, et al., Detection of a particle shower at the Glashow resonance with IceCube, Nature 591 (7849) (2021) 220–+.
[38] N. Aghanim, et al., Planck 2018 results-VI. Cosmological parameters, A&A 641 (2020) A6. doi:10.1051/0004-6361/201833910.
[39] I. Esteban, M. C. González-García, M. Maltoni, T. Schwetz, A. Zhou, The fate of hints: updated global analysis of three-flavor neutrino oscillations, JHEP 2020 (9) (2020) 1–22. doi:10.1007/JHEP09(2020)178.
[40] K. Asakura, et al., Study of electron anti-neutrinos associated with gamma-ray bursts using KamLAND, The Astrophysical Journal 806 (1) (2015) 87.
[41] S. Abe, et al., Search for Low-energy Electron Antineutrinos in KamLAND Associated with Gravitational Wave Events, The Astrophysical Journal 909 (2) (2021) 116.
[42] K. Abe, et al., Search for Neutrinos in Coincidence with Gravitational Wave Events from the LIGO–Virgo O3a Observing Run with the Super-Kamiokande Detector, The Astrophysical Journal 918 (2) (2021) 78. doi:10.3847/1538-4357/ac0d5a.
URL https://doi.org/10.3847/1538-4357/ac0d5a
[43] B. Baret, et al., Bounding the time delay between high-energy neutrinos and gravitational-wave transients from gamma-ray bursts, Astroparticle Physics 35 (1) (2011) 1–7.
[44] S. Fukuda, et al., Search for neutrinos from gamma-ray bursts using Super-Kamiokande, The Astrophysical Journal 578 (1)

(2002) 317.
[45] G. J. Feldman, R. D. Cousins, Unified approach to the classical statistical analysis of small signals, Phys. Rev. D 57 (1998) 3873–3889. doi:10.1103/PhysRevD.57.3873.
URL https://link.aps.org/doi/10.1103/PhysRevD.57.3873
[46] A. Strumia, F. Vissani, Precise quasielastic neutrino/nucleon cross-section, PhLB 564 (1-2) (2003) 42–54. doi:10.1016/S0370-2693(03)00616-6.
[47] M. Aartsen, et al., Observation and Characterization of a Cosmic Muon Neutrino Flux from the Northern Hemisphere using six years of IceCube data, The Astrophysical Journal 833 (1) (2016) 3.
[48] R. Abbasi, et al., IceCube high-energy starting event sample: Description and flux characterization with 7.5 years of data, Physical Review D 104 (2) (2021) 022002.
[49] M. Aartsen, et al., Measurements using the inelasticity distribution of multi-TeV neutrino interactions in IceCube, Physical Review D 99 (3) (2019) 032004.
[50] J. Stettner, Measurement of the diffuse astrophysical muon-neutrino spectrum with ten years of IceCube data, arXiv preprint arXiv:1908.09551 (2019).
[51] K. Hirata, et al., Observation in the Kamiokande-II detector of the neutrino burst from supernova SN1987A, Physical Review D 38 (2) (1988) 448. doi:10.1103/PhysRevD.38.448.
[52] D. N. Schramm, Neutrinos from supernova 1987A, Comments on Nuclear and Particle Physics 17 (5) (1987) 239–278.
[53] J. M. Lattimer, A. Yahil, Analysis of the neutrino events from supernova 1987A, The Astrophysical Journal 340 (1989) 426–434.